

INTRASURGICAL DYNAMICS OF MACULAR HOLE SURGERY

An Assessment of Surgery-Induced Ultrastructural Alterations with Intraoperative Optical Coherence Tomography

JUSTIS P. EHLERS, MD, DAVID XU, BS, PETER K. KAISER, MD, RISHI P. SINGH, MD, SUNIL K. SRIVASTAVA, MD

Purpose: To evaluate the intrasurgical retinal architectural and macular hole (MH) geometric alterations that occur during surgical MH repair using intraoperative optical coherence tomography.

Methods: A retrospective, multisurgeon, single-center, consecutive case series of 21 eyes undergoing surgical repair for MH with concurrent intraoperative optical coherence tomography using a custom microscope-mounted optical coherence tomography system was performed. All patients underwent surgical repair with pars plana vitrectomy, membrane peel, and gas tamponade. A novel three-dimensional segmentation algorithm was used for volumetric analysis of intrasurgical changes of MH geometry after surgical repair. Intraoperative optical coherence tomographic characteristics analyzed included MH volume, minimum diameter, base area, and hole height. Outer retinal architecture changes were analyzed both quantitatively and qualitatively.

Results: All 21 eyes were successfully imaged with intraoperative optical coherence tomography. Nineteen of 21 eyes had images of sufficient signal strength to allow for quantitative analysis. Significant changes were noted in MH geometry after internal limiting membrane peeling including increased MH volume, increased base area, and decreased top area (all $P < 0.03$). Additionally, increased subretinal hyporeflectance was noted by expansion of the height between the inner segment/outer segment and retinal pigment epithelium bands ($P = 0.008$). Peeling methods and surgeon experience did not correlate with the magnitude of architectural alterations. Macular hole algorithm measurements and alterations were associated with visual outcome and MH closure.

Conclusion: Significant alterations occur in MH geometry and outer retinal structure after internal limiting membrane peeling. These changes are subclinical and unable to be appreciated with en face surgical microscope viewing and require intraoperative optical coherence tomography for visualization. Preliminary analysis of these measurements identified an association with visual outcome and successful MH closure. The functional significance of these changes deserves further study.

RETINA 34:213–221, 2014

The development of macular hole (MH) surgery was a tremendous advance in the surgical management of this disease and for patient outcomes.¹ Significant enhancements to surgical technique, such as internal limiting membrane (ILM) peeling and facedown positioning, have dramatically improved anatomical success rates.^{2–4} However, extended gas tamponade and facedown positioning may have negative impact on patient satisfaction, quality of life,

and speed of visual recovery. In fact, many series now suggest that facedown positioning and/or extended gas tamponade may not be necessary in select patients.^{5–10} However, some of these series have not reached the >90% success rate that has been achieved with ILM peeling, facedown positioning, and gas tamponade.^{9,11,12} Identifying key factors that predict rapid hole closure could facilitate an individualized approach to patient care to maximize surgical

success while minimizing the necessity of facedown positioning and extended gas tamponade.

Spectral-domain optical coherence tomography has enabled high-resolution, in vivo, tomographic views of macular abnormality with dramatic impacts on the clinical care of vitreoretinal diseases.¹³ However, most optical coherence tomography (OCT) systems are table-top devices that evaluate the intraocular structures preoperatively and postoperatively. More recently, spectral-domain OCT has been adapted for intraoperative use, allowing for intrasurgical examination of anatomical changes before and after surgical maneuvers.^{14–20} Using intraoperative OCT (*iOCT*), novel findings have been described in numerous vitreoretinal diseases, including optic pit–related maculopathy, epiretinal membrane, MHs, retinal detachment, and retinopathy of prematurity.^{14,17–20}

The rapid, high-resolution, cross-sectional view provided by OCT is a natural complement to vitreoretinal surgery. Subclinical changes occurring during surgery may provide valuable information to the surgeon regarding surgical and postoperative management. Preliminary reports with *iOCT* suggest that changes in MH architecture occur after membrane peeling.^{18,20,21} Previous descriptions include changes in linear dimensions, changes in the hyporeflectivity band between the retinal pigment epithelium (RPE) and inner segment/outer segment (IS/OS) band, and alterations in the amount of subretinal fluid.^{18,20,21} Improved understanding of MH dynamics after membrane peeling may enhance our understanding of surgical outcomes, predict MH closure rates, and identify those patients who may not require extended tamponade or positioning. In-depth analysis of these architectural alterations that occur during surgery may provide key information to the surgeon regarding the necessity of positioning and gas tamponade to allow for image-guided customized surgical care.

In this study, we provide a high-resolution quantitative assessment of the impact of surgical maneuvers on MH architecture using *iOCT* and a novel automated segmentation algorithm that provides computer-aided segmentation of the entirety of the MH cavity. In addition, this

study examines the association of these architectural features with visual outcome and surgical success.

Methods

A retrospective, multisurgeon, single-center, consecutive case series was performed of eyes undergoing vitreoretinal surgical repair of MH with concurrent *iOCT* scanning at the Ophthalmic Imaging Center of the Cole Eye Institute. The study was approved by the Institutional Review Board of the Cleveland Clinic and adhered to the tenets of the Declaration of Helsinki.

Surgical Procedure

Standard 3-port 23-gauge or 25-gauge pars plana vitrectomy was performed by 3 surgeons (J.P.E., S.K.S., and P.K.K.) for MH repair. After completion of the core pars plana vitrectomy, dilute indocyanine green was used to stain the ILM and any epiretinal membrane, if present. The ILM was peeled in a circumferential pattern from around the edge of the MH in all cases. The peeling technique was surgeon's preference and included immediate engagement with vitreoretinal forceps or initial peel with a diamond-dusted membrane scraper with subsequent peeling with vitreoretinal forceps. After air–fluid exchange, perfluoropropane or sulfur hexafluoride was used to tamponade the MH. Gas selection was based on surgeon's preference. Patients adhered to strict facedown positioning for 1 week.

Intraoperative Optical Coherence Tomography Protocol

The Bioptigen SDOIS system (Bioptigen Inc, Research Triangle Park, NC) was attached to the surgical microscope with a custom microscope mounting system to allow for rapid and reproducible scanning using a custom microscope mount (Figure 1). Imaging was performed immediately before initiation of pars plana vitrectomy. Additionally, *iOCT* was performed after various surgical milestones based on surgeon preference and case characteristics (e.g., elevation of the posterior hyaloid, peeling of the ILM). A consistent image acquisition protocol was used including cubic 10 × 10 mm volume scans at 0° and 90°.

Volumetric Analysis

Intraoperative OCT data were exported for computer-aided analysis. Scans were initially examined for image quality. For inclusion, one of the volume scans was required to be of sufficient quality to allow for computerized volumetric analysis. Eyes with scan signal of insufficient quality for accurate assessment of MH

From the Ophthalmic Imaging Center, Cole Eye Institute, Cleveland Clinic, Cleveland, Ohio.

Supported by grants from Research to Prevent Blindness (R) (D.X. and P.K.K.).

Financial disclosures and possible conflicts: Bioptigen (P) (J.P.E. and S.K.S.), the Research to Prevent Blindness (R) (D.X. and P.K.K.), Carl Zeiss Meditec (C) (P.K.K. and R.P.S.), Topcon (C) (P.K.K.), Alcon (C) (P.K.K.), Novartis (C) (P.K.K.), Bausch and Lomb (C) (P.K.K. and S.K.S.), and Allergan (R) (S.K.S.).

None of the authors have any conflicting interests to disclose.

Reprint requests: Justis P. Ehlers, MD, Ophthalmic Imaging Center, Cole Eye Institute, Cleveland Clinic, 9500 Euclid Avenue, 132, Cleveland, Ohio 44195; e-mail: ehlersj@ccf.org

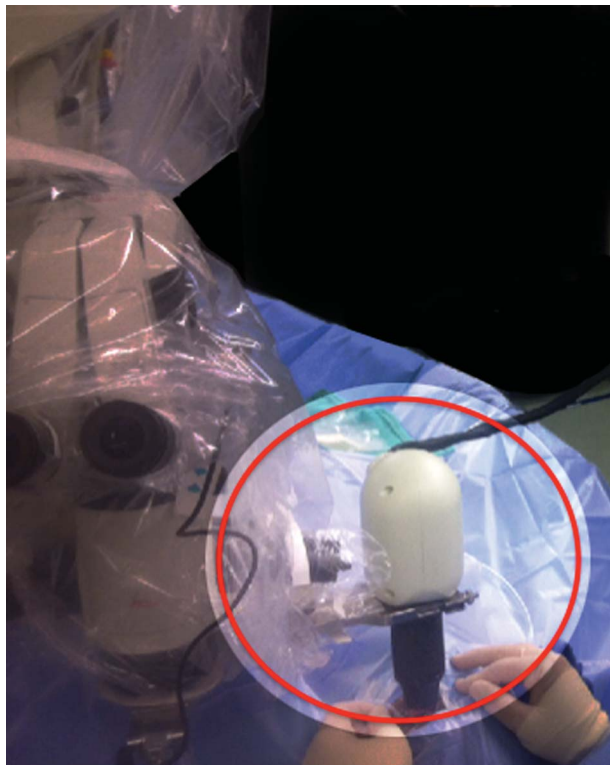


Fig. 1. Microscope-mounted iOCT system (red circle).

boundaries was excluded from the study. As previously described, the frame-by-frame B-scans were processed by a custom computerized algorithm that identified the optimal segmentation of the MH boundary using a graph searching technique, resulting in the delineation of the full-thickness hole cavity in every OCT frame.²² Each automated segmentation boundary was reviewed manually for accuracy. A three-dimensional surface representation of the MH was then generated. At each available surgical milestone, 7 measurements were calculated by the software (Figure 2) including MH volume (i.e., the summed voxel volume inside the MH boundary), MH base area (i.e., the area of polygon consisting of the

lateral edges of the MH boundary at the base of the hole), MH base diameter (i.e., the maximal diameter between lateral edges of the boundary at the base of the hole), the top area (i.e., the area of the polygon consisting of the lateral edges of the MH boundary at the top of the hole), the top diameter (i.e., the maximal diameter between lateral edges of the boundary at the top of the hole), the minimum diameter (i.e., the minimum lateral extent of the MH in the frame with the largest base width), and the MH height (i.e., the average normal distance between the base and top of the boundary).

Quantitative/Qualitative Ultrastructural Analysis

Outer retinal alterations after ILM peeling were assessed qualitatively and quantitatively. Two independent expert reviewers reviewed each scan for three variables before and after ILM peeling: subretinal hyporeflectivity (i.e., expansion of the IS/OS to RPE distance), lateral subretinal hyporeflectance expansion, and focal full-thickness retinal elevation. Quantitative measurement of subretinal hyporeflectance expansion was performed using the landmarks of the middle of RPE boundary and the middle of photoreceptor IS/OS boundary. Two measurements were calculated: the IS/OS–RPE height and the width (e.g., lateral extent) of IS/OS expansion. At each milestone (i.e., preincision, posthyaloid elevation, and post-ILM peeling), the height between the middle of the IS/OS and RPE boundaries in the central spectral-domain OCT frame (e.g., the frame with the greatest subjective cross-sectional hole size) was manually measured immediately nasal and temporal of the MH base. The IS/OS–RPE height was averaged between the nasal and temporal measurement, and the preincision and post-ILM peel IS/OS–RPE height was compared using paired *t*-test. At each time point, the lateral extent of the subretinal hyporeflectance was calculated by manually marking the most nasal and temporal edge where subretinal hyporeflectance was

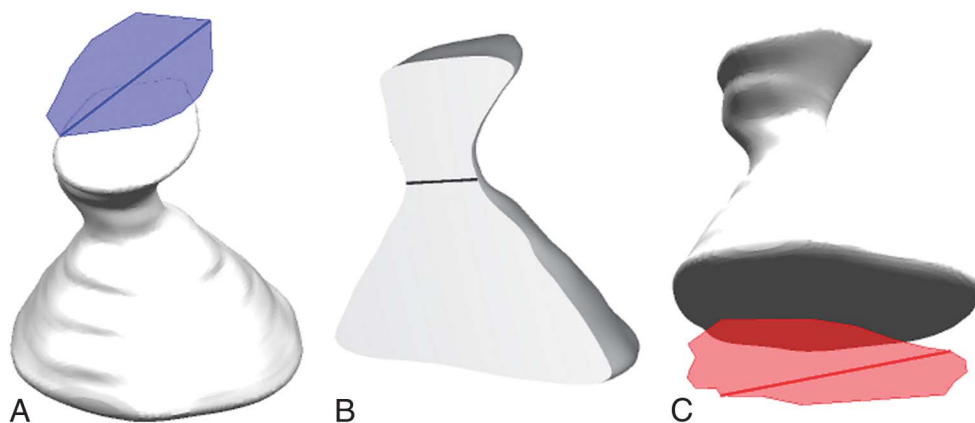


Fig. 2. Macular hole segmentation algorithm with three-dimensional reconstruction providing volume measurements and sample area/linear measurements: top area and diameter (A), minimum diameter (B), and base area and diameter (C).

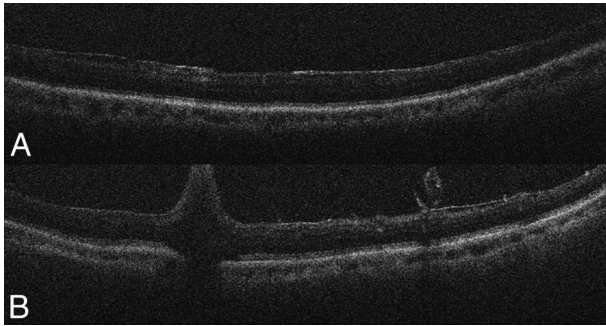


Fig. 3. Case example of focal full-thickness retinal elevation at the site of initiation of membrane peeling. **A.** Before ILM peeling. **B.** After ILM peeling with curled ILM and area of focal elevation of the retina.

seen in the central spectral-domain OCT frame. Then, the distance between the nasal and temporal edges was calculated measuring along the arc of the RPE.

Clinical/Surgical Analysis and Intraoperative Optical Coherence Tomography Correlation

Clinical and demographic patient details including MH stage using the Gass Classification, surgical technique for peeling, and MH closure were obtained from the chart. Surgical technique and primary surgeon (e.g., surgeon experience) correlated with quantitative outcomes.

Statistical analysis was performed to compare each MH measurement and outer retinal measurement between the preincision and post-ILM peel time points, preincision and posthyaloid removal time points, and posthyaloid removal and post-ILM peel time points by paired *t*-test. Multivariate logistic regression analysis was performed comparing these measurements with clinical/surgical factors. The Wilcoxon rank sum and Spearman rank correlation tests were used to analyze the association of MH measurements with MH closure and visual acuity, respectively.

Results

Clinical Characteristics

Twenty-one eyes of 21 patients were identified that underwent pars plana vitrectomy for idiopathic full-thickness MH with *i*OCT scanning. However, 2 eyes had scan quality below the threshold for accurate assessment and were excluded, leaving 19 eyes for analysis. The mean ± standard deviation patient age was 67 ± 9 years. Eighteen eyes underwent 23-gauge vitrectomy, whereas 1 eye underwent 25-gauge vitrectomy. Eight of 19 eyes had concomitant epiretinal membrane verified on OCT. Sulfur hexafluoride (n = 15) and perfluoropropane (n = 4) were used for gas tamponade. Mean preoperative visual acuity was 20/167 Snellen

Table 1. Macular Hole Measurements (Mean ± Standard Deviation) at the Preincision and Post-ILM Peel Time Points

	Volume, mm ³	Base Area, mm ²	Base Diameter, μm	Top Area, mm ²	Top Diameter, μm	Minimum Diameter, μm	Hole Height, μm	IS/OS-RPE Height, μm	SRHR Width, mm	Sample Size
Preincision (A)	0.140 ± 0.116	0.576 ± 0.462	1007 ± 427	0.391 ± 0.360	783 ± 373	285 ± 170	440 ± 120	39.4 ± 7.5	1.15 ± 0.41	19
Post-ILM peel (C)	0.160 ± 0.129	0.780 ± 0.596	1261 ± 476	0.202 ± 0.178	617 ± 332	317 ± 173	448 ± 148	49.5 ± 11.2	3.97 ± 3.00	19
Pairwise difference (% change)	0.020 (14)	0.205 (35)	254 (25)	-0.189 (-48)	-166 (-21)	32 (11)	7.8 (1.8)	10.1 (26)	2.83 (245)	
Significance	0.026	0.0021	0.0003	0.017	0.078	0.30	0.71	0.0002	0.0007	

SRHR, subretinal hyporeflectivity.

equivalent (mean logarithm of the minimum angle of resolution \pm standard deviation, 0.92 ± 0.60). Postoperatively, the mean visual acuity significantly improved to 20/61 Snellen equivalent (mean logarithm of the minimum angle of resolution \pm standard deviation, 0.49 ± 0.37) ($P = 0.0003$). Seventeen of 19 holes (89%) were successfully closed after surgical repair.

Qualitative Intraoperative Optical Coherence Tomography Analysis

Intraoperative OCT imaging was performed in all eyes immediately before surgical incision (i.e., preincision) and after ILM peeling (i.e., post-ILM). All 19 eyes had preincision and post-ILM peeling *i*OCT scans. Five of 19 eyes had *i*OCT performed after hyaloid elevation. Qualitative examination of *i*OCT scans was performed by two masked independent graders. Prominent subretinal hyporeflectance was noted in none of the eyes on preincision scans compared with 8 of 19 eyes (42%) after ILM removal. Additionally, the width of the subretinal expansion extended significantly beyond the MH edge, typically ending at the transition zone between peeled and unpeeled ILM. Focal areas of full-thickness retinal elevation was noted in 1 of 19 eyes and corresponded to the sites of initiation of membrane peeling on surgical video review (Figure 3). The edge of the

unpeeled ILM could be visualized as a curled, inward-diving free edge of the ILM at the border of the peeled zone.

Quantitative Intraoperative Optical Coherence Tomography Analysis

Volumetric and area measurements were performed for 19 of 19 eyes for both preincision and post-ILM scans. Macular hole measurements are tabulated in Table 1. After ILM peeling, MH geometry was significantly altered including MH volume increasing by 0.020 mm^3 ($P = 0.026$), base area increasing by 0.205 mm^2 ($P = 0.0021$), base diameter increasing by $254 \mu\text{m}$ ($P = 0.0003$), and top area decreasing by 0.189 mm^2 ($P = 0.017$) (Figures 4 and 5). There was no statistically significant difference in top diameter, minimum diameter, and MH height. In the 5 eyes that had posthyaloid removal scans, there was a significant increase in base area after hyaloid removal (Table 2).

Outer retinal layer measurements were performed to assess the changes in subretinal hyporeflectance. After ILM peeling, the IS/OS-RPE height increased by a mean of $9.3 \mu\text{m}$ ($P = 0.0002$) (Figure 6). The lateral width of the subretinal hyporeflectance also significantly increased after ILM peeling (2.83 mm;

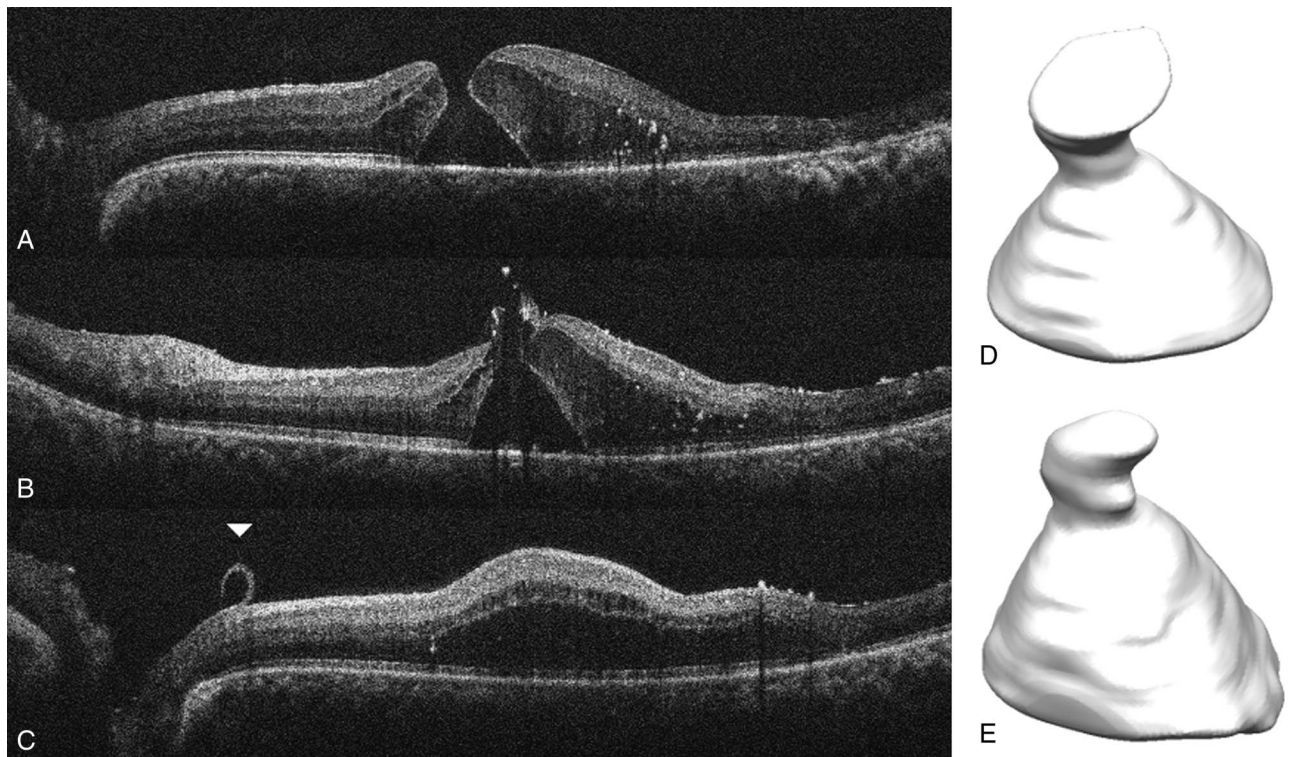


Fig. 4. Case example of intrasurgical changes in MH geometry with two-dimensional (A–C) and three-dimensional representation as documented with *i*OCT. Three-dimensional rendering of the preoperative (D) and post-ILM peel (E) scans demonstrating increased volume, increased base area, and decreased top area after ILM peeling.

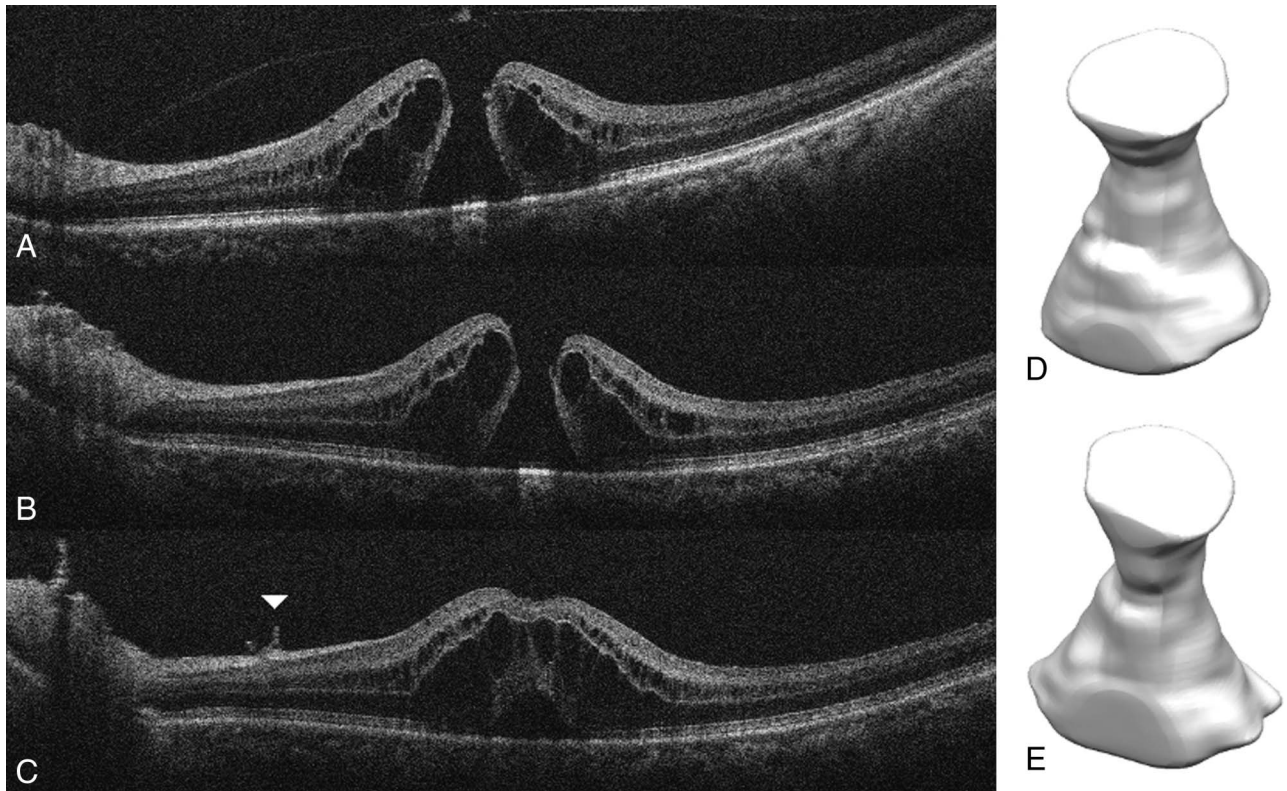


Fig. 5. Case 15. Stage 2 MH in a 77-year-old man with 20/400 preoperative acuity scanned at the preincision (A) and post-ILM (B and C) time points. The nasal border of the peeled ILM is clearly seen in the post-ILM peel cross-section inferior to the fovea (arrowhead). Three-dimensional rendering of the preoperative (D) and post-ILM peel (E) scans demonstrating a slight increase in base area and decrease in top area.

$P = 0.0007$). The geometric alteration in MH size and outer retinal architecture changes were compared among surgeons and peeling technique. There was no association of the magnitude of architectural alterations with specific surgeon, surgeon's experience, or the method of peeling (e.g., instrumentation used).

Preincision MH measurements significantly associated with preoperative vision included volume ($P = 0.03$), base area (0.001), base diameter (0.03), and IS/OS–RPE height (0.003) as significant features. Additionally, post-ILM peel scans revealed similar significant associations with preoperative vision, including MH volume ($P = 0.03$), base diameter ($P = 0.004$), and base area ($P = 0.001$). Final postoperative visual acuity was significantly associated with preincision base area ($P = 0.03$), preincision top area ($P = 0.002$), preincision IS/OS–RPE height ($P = 0.03$), post-ILM peel lateral extension of subretinal hyporeflectance ($P = 0.03$), and change in top area after ILM peel ($P = 0.004$). There was a trend toward an association with change in visual acuity after surgical repair and intraoperative change in IS/OS–RPE height after ILM peel ($P = 0.08$).

In this study, 2 of 19 MH failed to close after surgical repair. Univariate analysis of factors associated with MH closure identified several measurements that were

significantly associated with MH closure. The most significant variables associated with MH closure included MH volume (both preincision and post-ILM, $P = 0.01$), base area (both preincision and post-ILM, $P = 0.01–0.03$), base diameter (both preincision and post-ILM, $P = 0.01$), change in MH volume after ILM peeling ($P = 0.01$), change in top area (0.02), and change in base diameter ($P = 0.01$) (Table 3).

Discussion

Macular hole surgery has been revolutionized over the past few decades. Questions still remain regarding rate of hole closure, need for positioning, and necessity of prolonged gas tamponade. The ultrastructural impact of surgical manipulations on the retina and the long-term functional/structural impact of these changes have only been minimally explored. In this study, we present the largest *i*OCT case series of MH undergoing surgical repair. Additionally, this represents the first study to quantitatively assess the volumetric MH alterations associated with surgical maneuvers and the quantitative validation of the outer retinal changes associated with membrane peeling.

Table 2. Macular Hole Measurements (Mean ± Standard Deviation) at the Preincision and Posthyaloid Removal Time Points

	Volume, mm ³	Base Area, mm ²	Base Diameter, μm	Top Area, mm ²	Top Diameter, μm	Minimum Diameter, μm	Hole Height, μm	IS/OS-RPE Height, μm	SRHR Width, mm	Sample Size
Preincision (A)	0.091 ± 0.049	0.366 ± 0.237	823 ± 302	0.182 ± 0.166	487 ± 251	235 ± 104	446 ± 99	45.6 ± 5.3	1.08 ± 0.08	5
Posthyaloid removal (B)	0.098 ± 0.047	0.452 ± 0.300	1177 ± 235	0.189 ± 0.122	597 ± 190	233 ± 100	433 ± 103	42.2 ± 9.8	1.78 ± 0.94	5
Pairwise difference (% change)	0.007 (7.7)	0.086 (24)	354 (43)	0.007 (3.8)	110 (23)	-2 (-0.9)	-13 (-2.9)	-3.4 (-7.5)	0.70 (65)	
Significance	0.44	0.19	0.011	0.80	0.27	0.98	0.58	0.78	0.17	

SRHR, subretinal hyporeflectivity.

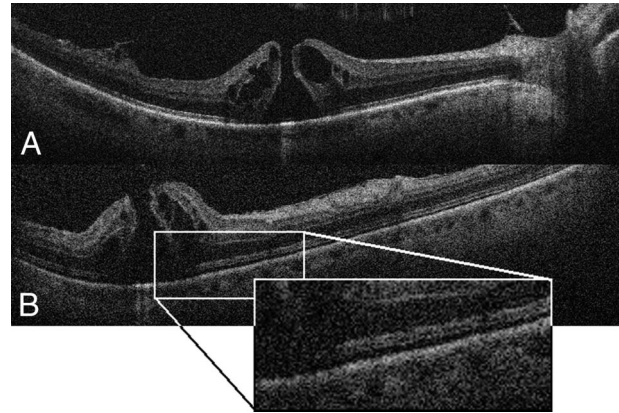


Fig. 6. Case example of outer retinal alterations with expansion of subretinal hyporeflectivity band between IS/OS junction and RPE. A. Before ILM peeling. B. After ILM peeling.

This study demonstrates significant alterations in MH geometry after surgical manipulation including increased MH volume, increase in base size (area and diameter), and decrease in top area. Ray et al¹⁸ examined 13 eyes undergoing surgical repair of MH with iOCT. In their report, they performed linear measurements of hole height and diameter and found a significant enlargement of base diameter without a change in MH height, consistent with the results of our study.¹⁸ Two additional small case series of five eyes also performed limited linear measurements of MH geometry. Dayani et al²⁰ noted a trend toward decreasing base diameter and no change in height. A second study²¹ demonstrated no change in base diameter and did not measure height. Given the small nature of these two studies, meaningful statistical analysis and comparison is difficult.

Ray et al¹⁸ also first described the phenomenon of increased subretinal hyporeflectance after membrane peeling for both MH and epiretinal membranes. To validate their findings, we elected to quantitatively and qualitatively assess the changes in outer retinal architecture after membrane peeling. Qualitative assessment of outer retinal changes showed prominent increased subretinal hyporeflectivity in 42% of eyes after ILM peeling. Additionally, quantitative analysis confirmed that in 17 of 19 eyes, there was an increase in the IS/OS-RPE height. The functional significance of these changes remains unclear and deserves further research. These changes may reflect photoreceptor stretching or even perhaps subclinical microneurosensory retinal detachments as posed by Ray et al¹⁸ To better assess these structural alterations, future studies should incorporate high-resolution functional testing (e.g., multifocal electroretinography, microperimetry) to provide improved correlation of structure and function. Although in this study, surgical technique was not associated with the

Table 3. Variables Associated With MH Closure

Preincision Measurements	Post-ILM Peel Measurements	Measurement Changes After ILM Peeling
MH volume ($P = 0.01$)	MH volume ($P = 0.01$)	Change in MH volume ($P = 0.01$)
Base area ($P = 0.01$)	Base area ($P = 0.03$)	Change in base diameter ($P = 0.01$)
Base diameter ($P = 0.01$)	Base diameter ($P = 0.01$)	Change in base area ($P = 0.03$)
Top area ($P = 0.02$)	Top area ($P = 0.02$)	Change in top area ($P = 0.02$)
Top diameter ($P = 0.05$)	Top diameter ($P = 0.02$)	Change in top diameter ($P = 0.02$)
Minimum diameter ($P = 0.04$)	Minimum diameter ($P = 0.03$)	Change in minimum diameter ($P = 0.03$)

magnitude of structural alterations, a large study may identify specific peeling techniques that may minimize the distortion of the outer retinal architecture. In this study, both IS/OS–RPE height and extension of subretinal hyporeflectance was significantly associated with postoperative visual acuity. In addition, there was a trend toward changes in IS/OS–RPE height after surgical manipulation and change in visual acuity. These functional/structural associations need further study in a larger prospective sample but provide important evidence of the potential utility of intraoperative examination of microarchitectural changes.

Volumetric segmentation and analysis of geometry was also associated with preoperative and postoperative visual acuity, including MH volume and base area. Importantly, change in top area after ILM peeling was also associated with postoperative visual acuity. This also supports the potential utility of real-time analysis of architectural changes and the potential prognostic value in these analyses.

Surgeons are continually trying to optimize the surgical experience and outcome for patients with MHs. With the current high anatomical successful closure rates, maximizing visual outcomes and the speed of recovery both become priorities. Some studies have suggested that minimal positioning and/or shorter gas tamponade can be successful in MH closure, particularly for small holes.⁵ Others have suggested using transtamponade OCT guidance for identifying hole closure.^{11,23} The rates of anatomical success in some of these studies are high, but the failure rates may not be satisfactory. The effect of intraoperative alterations in MH geometry on hole closure rate is unknown. More significant changes might reflect increase hole laxity and increased odds of closure. Alterations to specific dimensions (e.g., volume, height to base ratio) may also have an impact on hole closure rates. In this study, a 90% MH closure rate was achieved. The holes that did not close had a significantly higher MH volume and base area compared with those holes that closed. Additionally, changes in geometric features (e.g., MH volume, base diameter, top area) after ILM peeling were also associated with MH closure rate. These factors need further study

to help determine whether individualized approach to MH surgery would be feasible based on intraoperative MH characteristics and geometric configurations noted with *i*OCT. We are currently examining these features in our PIONEER study, a prospective *i*OCT study. In PIONEER, eyes with MH undergo *i*OCT imaging and subsequently undergo transtamponade imaging at 1 hour and 1 day postoperatively. Using the PIONEER protocol, we plan to carefully examine the correlation between intraoperative MH architecture changes and rate of MH closure in the early perioperative period.

There are several limitations to this study including its retrospective study design. Although this is a largest series to date, the sample size is still relatively small. Given the retrospective nature of the study, early structural/functional correlation to intraoperative findings was not possible. Additionally, posthyaloid *i*OCT imaging was limited to a small number of eyes, which may have provided additional information regarding the architectural changes that occur during vitrectomy surgery for MH.

This study confirms the feasibility of *i*OCT imaging during MH surgery and provides important evidence that significant architectural changes occur in MH geometry and outer retinal structure during surgical repair. This study also supports the novel application of software algorithms designed specifically for intraoperative applications (e.g., MH segmentation algorithm). This provides an objective and quantitative method of change analysis that may be able to further integrated to real-time *i*OCT in the future. Finally, this study provides early evidence to suggest that *i*OCT may provide important information regarding visual outcome and surgical success. The impact of these changes on the speed of hole closure and functional outcomes deserve further research.

Key words: optical coherence tomography, intraoperative, intrasurgical, macular hole, retinal surgery, intraoperative OCT.

References

1. Kelly NE, Wendel RT. Vitreous surgery for idiopathic macular holes. Results of a pilot study. *Arch Ophthalmol* 1991;109:654–659.

2. Kadosono K, Itoh N, Uchio E, et al. Staining of internal limiting membrane in macular hole surgery. *Arch Ophthalmol* 2000;118:1116–1118.
3. Haritoglou C, Reiniger IW, Schaumberger M, et al. Five-year follow-up of macular hole surgery with peeling of the internal limiting membrane: update of a prospective study. *Retina* 2006;26:618–622.
4. Lois N, Burr J, Norrie J, et al. Internal limiting membrane peeling versus no peeling for idiopathic full-thickness macular hole: a pragmatic randomized controlled trial. *Invest Ophthalmol Vis Sci* 2011;52:1586–1592.
5. Yorston D, Siddiqui MA, Awan MA, et al. Pilot randomised controlled trial of face-down posturing following phacovitrectomy for macular hole. *Eye (Lond)* 2012;26:267–271.
6. Almeida DR, Wong J, Belliveau M, et al. Anatomical and visual outcomes of macular hole surgery with short-duration 3-day face-down positioning. *Retina* 2012;32:506–510.
7. Chandra A, Charteris DG, Yorston D. Posturing after macular hole surgery: a review. *Ophthalmologica* 2011;226:3–9.
8. Dhawahir-Scala FE, Maino A, Saha K, et al. To posture or not to posture after macular hole surgery. *Retina* 2008;28:60–65.
9. Lange CA, Membrey L, Ahmad N, et al. Pilot randomised controlled trial of face-down positioning following macular hole surgery. *Eye (Lond)* 2012;26:272–277.
10. Malik A, Dooley I, Mahmood U. Single night postoperative prone posturing in idiopathic macular hole surgery. *Eur J Ophthalmol* 2012;22:456–460.
11. Eckardt C, Eckert T, Eckardt U, et al. Macular hole surgery with air tamponade and optical coherence tomography-based duration of face-down positioning. *Retina* 2008;28:1087–1096.
12. Tornambe PE, Poliner LS, Grote K. Macular hole surgery without face-down positioning. A pilot study. *Retina* 1997;17:179–185.
13. Chen TC, Cense B, Pierce MC, et al. Spectral domain optical coherence tomography: ultra-high speed, ultra-high resolution ophthalmic imaging. *Arch Ophthalmol* 2005;123:1715–1720.
14. Ehlers JP, Kernstine K, Farsiu S, et al. Analysis of pars plana vitrectomy for optic pit-related maculopathy with intraoperative optical coherence tomography: a possible connection with the vitreous cavity. *Arch Ophthalmol* 2011;129:1483–1486.
15. Ehlers JP, Tao YK, Farsiu S, et al. Integration of a spectral domain optical coherence tomography system into a surgical microscope for intraoperative imaging. *Invest Ophthalmol Vis Sci* 2011;52:3153–3159.
16. Ehlers JP, Tao YK, Farsiu S, et al. Visualization of real-time intraoperative maneuvers with a microscope mounted spectral domain optical coherence tomography system. *Retina* 2013;33:232–236.
17. Lee LB, Srivastava SK. Intraoperative spectral-domain optical coherence tomography during complex retinal detachment repair. *Ophthalmic Surg Lasers Imaging* 2011;42:e71–e74.
18. Ray R, Baranano DE, Fortun JA, et al. Intraoperative microscope-mounted spectral domain optical coherence tomography for evaluation of retinal anatomy during macular surgery. *Ophthalmology* 2011;118:2212–2217.
19. Binder S, Falkner-Radler CI, Hauger C, et al. Feasibility of intrasurgical spectral-domain optical coherence tomography. *Retina* 2011;31:1332–1336.
20. Dayani PN, Maldonado R, Farsiu S, Toth CA. Intraoperative use of handheld spectral domain optical coherence tomography imaging in macular surgery. *Retina* 2009;29:1457–1468.
21. Hayashi A, Yagou T, Nakamura T, et al. Intraoperative changes in idiopathic macular holes by spectral-domain optical coherence tomography. *Case Rep Ophthalmol* 2011;2:149–154.
22. Xu D, Yuan A, Kaiser PK, et al. A novel segmentation algorithm for volumetric analysis of macular hole boundaries identified with optical coherence tomography. *Invest Ophthalmol Vis Sci* 2013;54:163–169.
23. Masuyama K, Yamakiri K, Arimura N, et al. Posturing time after macular hole surgery modified by optical coherence tomography images: a pilot study. *Am J Ophthalmol* 2009;147:481–488, e2.